Geophysical Research Letters

RESEARCH LETTER
10.1029/2024GL111229

Refined Estimates of Global Ocean Deep and Abyssal Decadal Warming Trends

Gregory C. Johnson[1] **and Sarah G. Purkey**[2]

[1]NOAA Pacific Marine Environmental Laboratory, Seattle, WA, USA, [2]Scripps Institution of Oceanography, University of California San Diego, La Jolla, CA, USA

Key Points:

- Analysis of Deep Argo float and historical ship-based CTD data reveal global patterns in deep and abyssal layer decadal temperature trends
- High resolution maps reveal spreading of abyssal warming from Antarctica and cooling from the North Atlantic on sub-basin spatial scales
- Globally integrated decadal heat content trends are 21.6 (±6.5) TW in the deep and 12.9 (±1.8) TW in the abyssal layer

Supporting Information:

Supporting Information may be found in the online version of this article.

Correspondence to:

G. C. Johnson,
gregory.c.johnson@noaa.gov

Citation:

Johnson, G. C., & Purkey, S. G. (2024). Refined estimates of global ocean deep and abyssal decadal warming trends. *Geophysical Research Letters*, *51*, e2024GL111229. https://doi.org/10.1029/2024GL111229

Received 5 JUL 2024
Accepted 12 SEP 2024

Author Contributions:

Conceptualization: Gregory C. Johnson
Data curation: Gregory C. Johnson
Formal analysis: Gregory C. Johnson
Funding acquisition: Gregory C. Johnson, Sarah G. Purkey
Methodology: Gregory C. Johnson
Project administration: Gregory C. Johnson, Sarah G. Purkey
Resources: Gregory C. Johnson
Software: Gregory C. Johnson
Validation: Gregory C. Johnson
Visualization: Gregory C. Johnson, Sarah G. Purkey

Abstract Deep and abyssal layer decadal temperature trends from the mid-1980s to the mid-2010s are mapped globally using Deep Argo and historical ship-based Conductivity-Temperature-Depth (CTD) instrument data. Abyssal warming trends are widespread, with the strongest warming observed around Antarctic Bottom Water (AABW) formation regions. The warming strength follows deep western boundary currents transporting abyssal waters north and decreases with distance from Antarctica. Abyssal cooling trends are found in the North Atlantic and eastern South Atlantic, regions primarily ventilated by North Atlantic Deep Water (NADW). Deep warming trends are prominent in the Southern Ocean south of about 50°S, the Greenland-Iceland-Norwegian (GIN) Seas and the western subpolar North Atlantic, with cooling in the eastern subpolar North Atlantic and the subtropical and tropical western North Atlantic. Globally integrated decadal heat content trends of 21.6 (±6.5) TW in the deep and 12.9 (±1.8) TW in the abyssal layer are more certain than previous estimates.

Plain Language Summary Even the deepest waters in the ocean, which sink to the abyss around Antarctica after being cooled and made saltier by heat exchange with the atmosphere and sea ice formation, have been shown to be warming around much of the globe in recent decades. The net warming rate below 2000-m depth accounts for about 10% of total ocean heat uptake, but uncertainties in prior estimates have been about half the size of the signal owing to sparse sampling in the deep ocean. However, new observations from Deep Argo floats, capable of profiling to the ocean floor in most locations, have improved that situation in some regions. Here we analyze these new observations together with historical observations collected from ships since the 1970s to map decadal ocean temperature trends around the globe. As a result, we use more historical data than previous estimates. We refine the local patterns of warming and cooling in the waters deeper than 2,000 m. We confirm the amplitude of the net warming below 2,000 m estimated in previous studies, and extend the time covered by those estimates. The increased data coverage substantially reduces the uncertainty of the net warming estimate.

1. Introduction

The oceans have taken up around 89% of the excess heat entering the climate system over the past several decades as a result of the human-caused buildup of greenhouse gasses in the atmosphere (von Schuckmann et al., 2023). The full-depth ocean warming rate, estimated at between 332 and 403 TW from 1993 through 2023 (Johnson et al., 2024) includes about 36 (±16) TW for the deep (2,000–4,000 m) and abyssal (4,000–6,000 m) layers of the ocean. This build-up of heat in the oceans causes sea level rise through the steric expansion of sea water and by increasing melt rates of marine-terminating ice sheets. In addition, ocean warming decreases sea ice coverage which decreases Earth's albedo, strengthens tropical cyclones, warms and increases the moisture content of the atmosphere which intensifies the hydrological cycle, and causes marine heatwaves which can have devastating impacts on ecosystems such as coral reef bleaching (IPCC, 2021).

Argo, an international global array of autonomous profiling CTD-instrument-equipped floats presently numbering almost 4,000, each profiling once every 10 days, monitors the spatial and temporal patterns of change in temperature and salinity in near real time in the upper 2,000 dbar (~2,000 m) of the ocean. It has revolutionized our understanding of ocean physics (Johnson et al., 2022; Roemmich et al., 2019). The array first reached sparse global coverage around 2005. Since then it has greatly reduced uncertainty in upper ocean warming trends (Johnson et al., 2016).

Writing – original draft: Gregory C. Johnson
Writing – review & editing: Gregory C. Johnson, Sarah G. Purkey

However, the oceans below the 2000-dbar pressure limit of Core Argo floats remain sparsely sampled in space and time, primarily by oceanographic research vessels occupying what are customarily referred to as hydrographic sections, where CTDs are lowered from the sea surface to the sea floor or some intermediate depths at intervals along the ship's path. Global observational studies have used repeat hydrographic section data to quantify abyssal and deep ocean temperature trends regionally and globally (Purkey & Johnson, 2010). Other studies have used residual calculations based on sea level budgets, energy budgets, or both (Storto et al., 2022; Volkov et al., 2017), and assimilation output (Wunsch & Heimbach, 2014). In the few historically well-sampled regions more has been done to look at both decadal trends and interannual variability. The Labrador Sea, where a major component of NADW, called Labrador Sea Water, is formed is one prominent example, where the depth, temperature, and salinity of wintertime mixed layers, and hence the volume and water properties of Labrador Sea Water formed, has varied interannually (Yashayaev & Loder, 2016) leading to changes in deep ocean heat conent (Desbruyères et al., 2014). However, in most other locations in situ oceanographic data have been too sparse to estimate much more than large spatial-scale and decadal time-scale trends.

A global Deep Argo array has been proposed (Johnson et al., 2015; Roemmich et al., 2019) as part of OneArgo to extend Argo's spatial coverage to the sea floor. The first Deep Argo regional pilot array was begun in the Southwest Pacific Basin in 2016, with basin-scale arrays now established in the Brazil, Argentine, North Atlantic, and Australia-Antarctic basins, with additional floats in the Indian Ocean and North Pacific (Zilberman et al., 2023). Combining data from Deep Argo Regional Pilot arrays and historical ship-based surveys have allowed for assessment of decadal abyssal and deep ocean warming trends with much smaller uncertainties than previous estimates (Johnson et al., 2019, 2020). These assessments have mostly been of basin averages, although spatial patterns in the warming trends have been detected in the Argentine Basin, with faster warming at the southern boundary in the deepest pressures, consistent with a slow-down of westward inflow of AABW at the southern boundary of that basin (Johnson, 2022).

Here, for the first time, we use all available historical ship-based and Deep Argo CTD data to examine the global distribution of anthropogenic heat in the deep and abyssal ocean. The increase in data from Deep Argo resolves spatial patterns on sub-basin scales, providing new insight into the vertical and horizontal distribution of deep warming (Section 3). Using the mapped global deep trends, we calculate new global inventories of deep and abyssal warming trends, with uncertainties substantially reduced compared with previous estimates.

2. Data and Methods

We downloaded Deep Argo CTD data from a Argo Global Data Assembly Center (Argo, 2024) on 3 May 2024, using delayed-mode and real-time adjusted pressure, temperature, and salinity data with quality flagged as 1 (good) or 2 (probably good). We downloaded high-resolution ship-based CTD data from the World Ocean Database for all profiles extending at least to 2,100 m on 2 May 2024, again using only data flagged as "good". Deep Argo accuracy targets of ± 0.002 g kg^{-1}, ± 0.001°C, and ± 3 dbar (Zilberman et al., 2023) are similar to those for global shipboard CTD work (Sloyan et al., 2019), well below geophysical "noise" levels (e.g., mesoscale eddy and internal wave variability) for this analysis.

We calculated absolute salinity (S_A) and conservative temperature (C_T) for all of the CTD profiles using the GSW TEOS-10 toolbox (McDougall & Barker, 2011). We linearly interpolated all the profiles to a uniform 10-dbar pressure grid. We discarded values that were interpolated over pressure spans exceeding 100 dbar. These steps resulted in 66,617 ship-based CTD profiles and 30,169 Deep Argo CTD profiles that reached at least 2,100 dbar, with counts decreasing steadily with increasing pressure for each data set to 1,020 and 1268, respectively, by 6,000 dbar.

We sorted the profiles into ~167 × 167 km bins to calculate trends in C_T. The sides of these bins are 1.5° of latitude and 1.5° of longitude in length on the equator, but their widths in longitude increase with increasing latitude owing to the approximately spherical geometry of the Earth. This bin size is chosen both to be small enough to minimize noise from spatial gradients and to match the deep temperature spatial decorrelation scale estimated from oceanographic section data (Purkey & Johnson, 2010), making each bin statistically independent in terms of estimating degrees of freedom. If there were two or more C_T values with the final and initial year separated by at least a decade on a pressure level within a bin, we estimated the temporal trend, $\partial C_T/\partial t$, from the slope of a least squares linear fit of C_T versus time (t), determined the C_T value at 1 January 1995 from the fit, and also stored the times of the initial and final data point used in the fit.

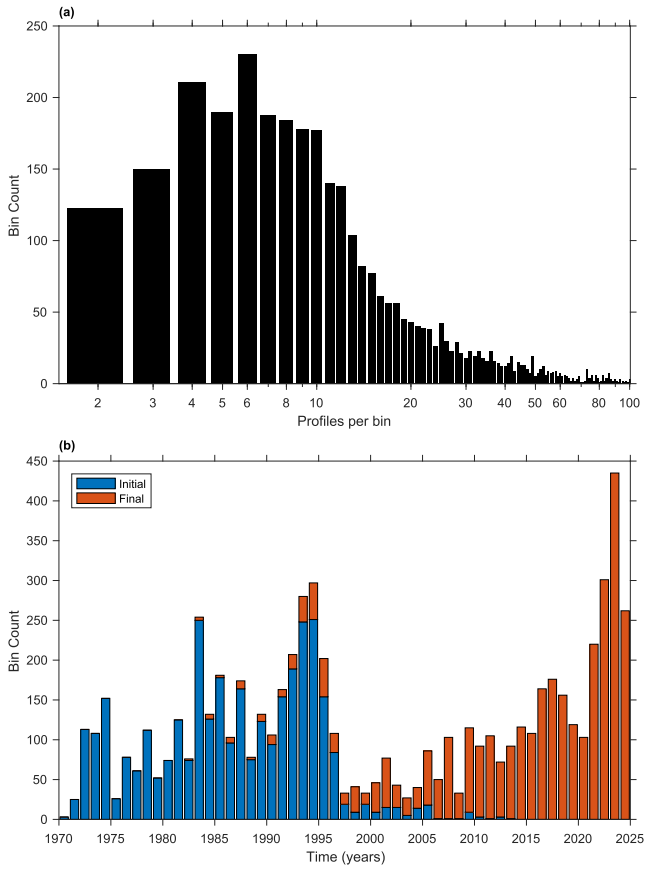

Figure 1. (a) Histogram of number of profiles per 167 × 167 km bin at 2,100 dbar, with from 2 to 100 shown. Of the 3,338 bins with 2 or more retained profiles, 91 have profile counts exceeding 100, the maximum being 542. (b) Histogram of initial (blue) and final (orange) years of trends in bins at 2,100 dbar.

We discarded (a very few) extreme outliers of $\partial C_T/\partial t$ (and accompanying variables) using the following procedure: At each pressure level we sorted all of the data into 34 deep basins (the 33 used by Purkey and Johnson (2010) with a 34th added for the GIN seas). Following Tukey (1977) we computed the first and third quartiles of $\partial C_T/\partial t$ for each basin, subtracted the first from the third to find the interquartile range, and discarded any values that were less than the first quartile minus 3 times that range or greater than the third quartile plus three times that range. This quality control step left 70,731 profiles in 3,338 bins used to estimate trends at 2,100 dbar. Those numbers decreased steadily with increasing pressure to 850 profiles in 106 bins at 6,000 dbar. Numbers of profiles in each bin at 2,100 dbar ranged from 2 to 542 with a mode of 6 (Figure 1a).

The starting and ending years of the trends remaining after quality control varies by bin and a bit by depth. At 2,100 dbar, the bins' starting years are fairly evenly distributed through the 1970 and 1980s, with a substantial number in the early 1990s, and much fewer in the late 1990s to early 2010s (Figure 1b). A few bins' ending years occur in the 1980 and 1990s, with most in the 2020s. The mean starting year at 2,100 dbar is 1986 and increases to 1989 at 6,000 dbar. The mean ending year at 2,100 dbar is 2015 and increases to 2017 at 6,000 dbar.

To convert remaining values into rates of change of ocean heat content (in W) we smoothed ETOPO1 bathymetry (Amante & Eakins, 2009; NOAA National Geophysical Data Center, 2009) with a two-dimensional Hanning filter with 0.25° latitude × 0.25° longitude half-power points and subsampled it at 0.125° × 0.125° intervals. We then used TEOS-10 to convert those depths to pressure, and estimated the ocean mass in each 10-dbar layer for each bin using that data set and a nominal gravitational acceleration value of $g = 9.8$ m s^{-2}. While the number of bins sampled decreased with increasing pressure, the fraction of the ocean area sampled in each 10-dbar pressure bin was relatively constant, dropping from 29% at 2,100 dbar to 25% at 6,000 dbar. When vertically integrated these bins sample 27% of the ocean mass below 2,000 dbar.

Once the extreme outliers were removed, we used the remaining values of $\partial C_T/\partial t$ and other analyzed variables at each pressure level to interpolate spatially to the bins without direct estimates using the natural neighbor option in the Matlab griddata interpolation algorithm. It uses a local weighted average of nearby direct estimates of $\partial C_T/\partial t$ to interpolate values of $\partial C_T/\partial t$ for bins in which a direct estimate is missing. We used the binned bathymetry to remove interpolated values of $\partial C_T/\partial t$ in locations where they were deeper than the bathymetry. We then used the TEOS-10 value of the specific heat of seawater for conservative temperature, $c = 3{,}991.8680$ J kg^{-1}°C^{-1}, times $\partial C_T/\partial t$ and the ocean mass to estimate time rates of ocean heat content change, in units of W.

To estimate uncertainties in globally integrated rates of change of ocean heat content, we computed the standard deviation of $\partial C_T/\partial t$ in each pressure layer for only the bins in which an estimate was made directly from data. We assumed each bin provided a degree of freedom, and computed 5–95% confidence intervals (90% two-tailed) using the standard deviations and the degrees of freedom estimated as detailed above, assuming Student's t-distribution. We then converted those into heat content change using the mass of the global ocean in that layer using the same methods as described just above. When summing vertically over layers, we assumed that errors were perfectly correlated, and thus added uncertainties for each layer to get the summed uncertainty. We make this assumption since eddy signatures and aliasing of spatial gradients introduced when binning data likely dominate the uncertainties, and both of those noise sources are likely to be strongly correlated in the vertical. To the extent that this assumption is too strong, uncertainty estimates may be conservative (e.g., larger than actual uncertainties).

For comparison, we also update basin-average deep (2,000–4,000 dbar) and abyssal (4,000–6,000 dbar) temperature and heat content trend estimates following (Purkey & Johnson, 2010), but using only repeat hydrographic

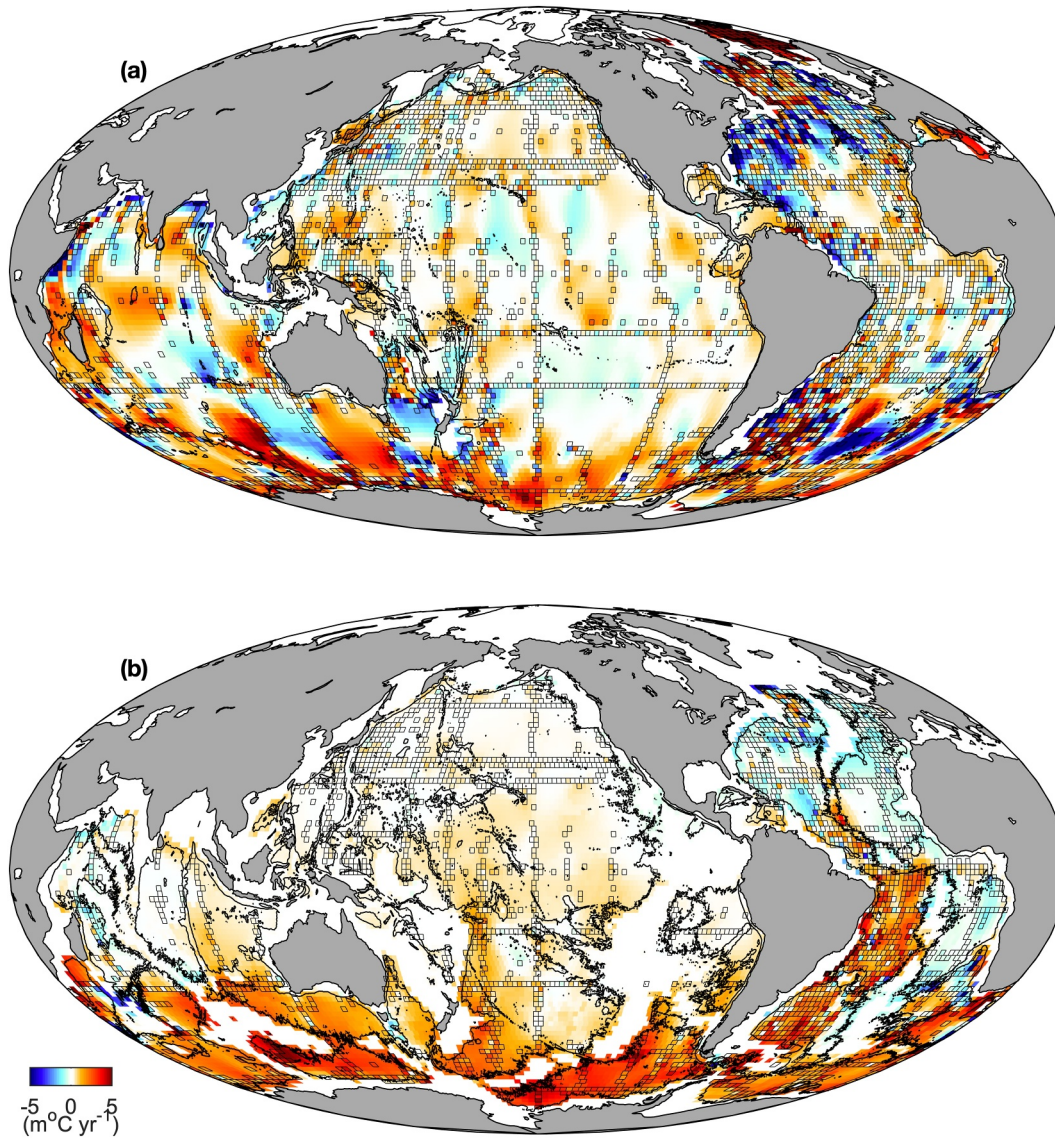

Figure 2. Map of (a) deep (2,000–4,000 dbar) and (b) abyssal (4,000–6,000 dbar) pressure-averaged decadal temperature trends in 167 × 167 km bins with the 2,000 and 4,000 dbar isobars of bottom bathymetry contoured, respectively (black lines). Bins with directly measured trends are bordered by light black lines, with the remaining bins values interpolated by natural neighbor.

section data available at https://cchdo.ucsd.edu/ as of January 2024 (Figures S1 and S2 in Supporting Information S1).

3. Results

The spatial distribution of local abyssal (4,000–6,000 dbar) temperature trends (Figure 2b) shows the strongest warming trends adjacent to Antarctica with the warming extending northward through much of the global oceans, generally weakening with distance from Antarctica. Abyssal cooling is found mostly in both the eastern and western deep basins of the North Atlantic as well as the Angola Basin in the eastern South Atlantic. The deep (2,000–4,000 dbar) temperature trend map (Figure 2a) again shows mostly warming around Antarctica, but more patchy regions of both warming and cooling to the North, with notable warming trends in the Greenland-Iceland-Norwegian Seas and much of the Subpolar North Atlantic, and a notable region of strong cooling throughout much of the rest of the western North Atlantic. Despite the patchiness in the deep layer, with especially strong

variability around and just to the north of the Antarctic Circumpolar Current, the warming trend dominates the global integral for the deep layer, as we quantify below.

The strength of the local abyssal warming (Figure 2b) diminishes with distance along the spreading paths of AABW from its formation sites. The strongest warming is seen within the Ross Gyre, directly downstream of the Ross Shelf, and the Australian-Antarctic Basin, directly downstream from Cape Adare (both AABW formation regions) with warming rates of 3–4 m°C yr^{-1}. South of the Antarctic-Pacific Rise, the warming rate decreases slightly to the east outside of the Ross Gyre over the Bellingshausen Plain, consistent with previously reported patterns of warming and freshening (Purkey et al., 2019).

In the western South Atlantic, the strong abyssal warming trend of 2 m°C yr^{-1} seen in the Weddell Basin adjacent to another AABW formation region remains strong and largely undiminished through the Argentine and Brazil Basins. Warming rates vary little across the Argentine and Brazil basins despite almost complete data coverage. This warming trend extends across the equator into the western basin of the North Atlantic to about 15°N along the western flank of the Mid-Atlantic Ridge, albeit somewhat diminished. In the Southeastern Atlantic, the Cape Basin shows patchy warming and cooling trends.

In the Pacific and Indian oceans, the abyssal layer temperature trends (Figure 2b) are the strongest along the two deep western boundary currents transporting AABW to the north. In the Southwest Pacific Basin, the abyssal warming trend is strongest following this current around the Campbell Plateau, south and east of New Zealand, but remains relatively large on the western margin of that basin all the way to the Samoan Passage at 10°S. The warming generally decreases eastward across the basin away from the boundary. To the north, in the Central Pacific Basin, warming is more moderate and diffuse through the basin, but relatively constant in magnitude almost as far north as Hawaii. To the west and north of Hawaii, the warming trend is weaker, and interspersed with small areas of weak cooling trends. In the far southwestern Pacific in the Tasman Basin and the far southeastern Pacific in the Chile Basin, moderate warming is observed with weakening warming through the Peru and Bauer basins to the north.

In the Indian Ocean, on the eastern side of the Weddell Gyre, the warming stays constant and the warming bleeds into the western Indian Ocean to the Crozet Basin. Further to the north, in the Madagascar, Mascarene, Somali, and Arabian basins, little warming is observed, with some patches of weak cooling as well. The strongest abyssal warming in the Indian Ocean is seen through the AABW pathway in the eastern portions of that ocean, east of the Southeast Indian and Ninetyeast Ridges (Figure 2b). The very strong warming seen in the Australian-Antarctic Basin continues into the South Australian and Wharton basins, decreasing to the north along this pathway, but still visible all the way to Indonesia. The Central Indian Basin exhibits very weak trends.

The North and Eastern Atlantic, which is mostly filled by NADW (Johnson, 2008), shows a very different pattern then the rest of the abyssal ocean. Cooling trends are observed through most of this region with some patchiness in the rate. In the very northern end of the North American Basin, some warming is observed, possibly reflecting the higher prevalence of recent data from Deep Argo taken over the last 5 years. East of the mid-Atlantic rise, weak abyssal cooling on the order of 0.3 m°C yr^{-1} is observed from far north all the way to the south end of the Angola Basin (Figure 2b).

Within the deep layer (2,000–4,000 dbar) local warming and cooling trends are generally larger with more spatial heterogeneity than in the abyssal layer (Figure 2a). Despite the patchiness, a few patterns are clear: First, strong mostly homogenous warming is observed throughout most of the deep Southern Ocean south of circa 50°S (the northern range of the Antarctic Circumpolar Current). Second, the GIN seas show a very strong warming trend of about 7 m°C yr^{-1}. Third, the western North Atlantic shows a strong bimodal pattern, with strong warming in the western portion of the subpolar gyre and cooling in the eastern portion of that gyre as well as western subtropical and tropical regions all the way to the equator. Fourth, the Pacific and Indian oceans both show patches of warming and cooling spread throughout, with smaller magnitudes in the Pacific but no obvious large-scale patterns. Finally, the region on the northern edge of the Antarctic Circumpolar Current exhibits strong patchy patterns of warming and cooling, likely induced by energetic eddies and shifting fronts.

Zonal averages of $\partial C_T/\partial t$ (Figure 3a) clearly show the strong abyssal and deep warming rates in the Southern Ocean. Zonal average warming rates generally decrease with increasing zonal average C_T from 0.0 to 1.0°C. North of about 10°N zonal average warming is weaker and limited to the lower half of the abyssal layer, and cooling (mostly in the Atlantic) is apparent in the zonal average. North of about 60°N the strong warming is

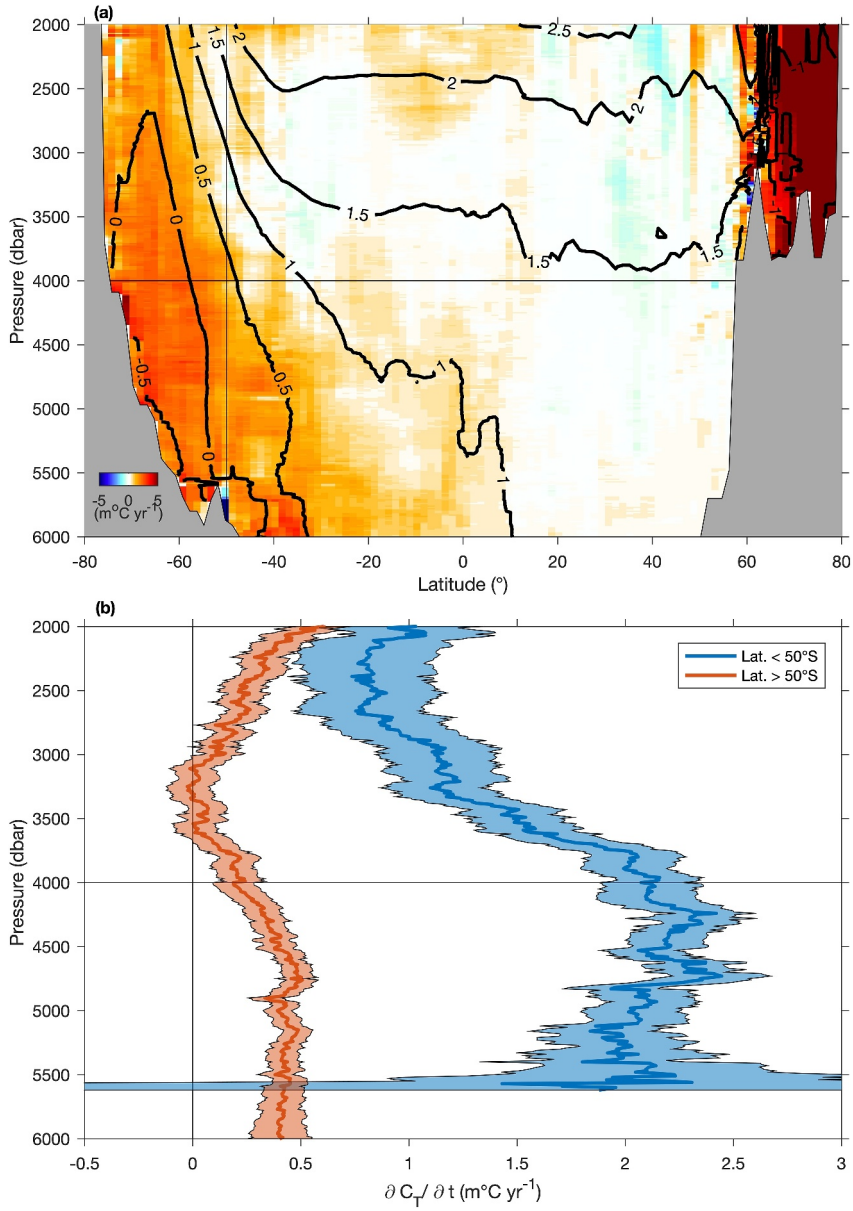

Figure 3. (a) Zonal average temperature trends (colorbar) versus latitude and pressure with zonal average Jan. 1995 temperatures contoured (black lines) at 0.5°C intervals. Thin black lines at 50°S and 4,000 dbar. (b) Mass averaged temperature trends (solid lines) with 5%–95% uncertainties (shading) for latitudes south of 50°S (blue) and north of 50°S (red). Thin black lines at 0 m°C yr^{-1} and 4,000 dbar.

mostly found in the GIN seas, but they have a very small area (Figure 2a) and so don't contribute substantially to the global average.

Given the strong warming signal seen in the Southern Ocean in both the abyssal and deep layers, and the weaker warming signal seen in the deep layer in the rest of the globe, we present mass-averaged temperature trends versus pressure north and south of 50°S (Figure 3b). South of 50°S, the average temperature trend in the abyssal layer is about 2 m°C yr^{-1}, and that trend weakens with decreasing pressure to around 1 m°C yr^{-1} at 2,800 dbar, where it remains to 2,000 dbar. North of 50°S, the average temperature trends are weaker at all pressures than south of that latitude, but with overall warming from 2000 to 6000 dbar, albeit everywhere at a rate below 0.5 m°C yr^{-1}, and indistinguishable from zero from about 3,100 to 3,600 dbar.

Globally integrated heat content trends in the deep layer (2,000–4,000 dbar) are 21.6 (±6.5) TW and in the abyssal layer (4,000–6,000 dbar) they are 12.9 (±1.8) TW. Summing these trends (and their uncertainties, since they are likely vertically correlated) and dividing by the surface area of the Earth, 510×10^{12} m^2, yields an average rate of energy gain of 0.068 (±0.016) W m^{-2} from 1987 to 2015, where the starting and ending years have also been mass-averaged globally.

4. Discussion

The sum of the globally integrated decadal heat content trends of 21.6 (±6.5) TW in the deep (2,000–4,000 dbar) and 12.9 (±1.8) TW in the abyssal layer (4,000–6,000 dbar) comes to 34.5 (±8.3) TW. An update of Purkey and Johnson (2010) trends through December 2023 (Johnson et al., 2024, see also Supporting Information S1), is similar in amplitudes, with 23.9 (±15.4) TW in the deep layer and 12.3 (±3.1) in the abyss summing to 36 (±19) TW. However, the trends we present here have about half of the uncertainties compared with those of the updated Purkey and Johnson (2010) trends because they rely on only repeat hydrographic data and we use all high vertical resolution CTD data so long as we have at least two profiles separated by a decade or more in time in a 167 × 167 km bin. Our use of these bins and Deep Argo profiles allows us to use much more data, sampling approximately 1/4 of the ocean mass directly. Even though we incur some aliasing of spatial gradients within those bins into our trend estimates, apparently bin averaging and including more data combine to more than offset the noise introduced by that aliasing.

Our mapping of the binned data, while simple, reveals some patterns within basins that were obscured in the Purkey and Johnson (2010) analysis, showing abyssal warming rates steadily decreasing with distance from Antarctica in multiple ocean basins (Figure 2b vs. Figure S1b in Supporting Information S1) and in the zonal average (Figure 3a). For instance, the greater warming of the abyssal water in the western portion of the Southwest Pacific Basin (Figure 2b) is very clear, and consistent with a reduction in northward flow of AABW estimated from the analyses of repeat hydrographic section data (Kouketsu et al., 2011), as is the warming of the abyssal layer in the low-latitude western north Atlantic Ocean on the western flank of the mid-Atlantic Ridge (Johnson et al., 2008).

The warming in much of the global ocean abyss can be attributed to reductions in the formation rate and density of AABW, with a signal communicated on decadal time-scales by planetary waves in regions distant from Antarctica, as far north as the North Pacific (Masuda et al., 2010). There is an extensive set of regional analyses of this warming (e.g., Gunn et al., 2023; Zhou et al., 2023; Silvano et al., 2023, and references therein). These changes have been attributed in modeling studies to freshening of dense shelf waters by increased melting rates of marine-terminating ice sheets in the Pacific and Indian sectors of the Southern Ocean (Fogwill et al., 2015; Li et al., 2023) and decreased sea-ice export arising from decadal natural wind variations in the Atlantic sector (Zhou et al., 2023). The three basins primarily fed by NADW even in the abyssal layer (Johnson, 2008), two in the North Atlantic and the Angola Basin, in the Eastern South Atlantic, are cooling consistent with previously observed long-term cooling of lower NADW (Mauritzen et al., 2012).

About 27% of the ocean mass is sampled from 2000 to 6000 dbar. The percentage area sampled at different pressures decreases only slightly with increasing pressure, despite the reduction in numbers and coverage of observations with increasing pressure, because the area of the ocean also decreases with increasing pressure. Nonetheless, there are also large variations in sampling among the different ocean basins. The North Atlantic and northern North Pacific are quite well sampled (Figure 2). The Brazil and Argentine Basins in the western South Atlantic are also very well sampled, because of the extensive historical ship-based data set in those regions coupled with the establishment of Deep Argo regional pilot arrays there. The rest of the ocean regions, especially the Indian, South Pacific, and Southern Oceans, are more sparsely sampled in the deep and abyssal layers.

The deep layer temperature trend map (Figure 2a), and zonal averages (Figure 3b) show strong warming trends south of 50°S. That dividing latitude is somewhat arbitrary, but only slightly north of the SubAntarctic Front of the Antarctic Circumpolar Current (Orsi et al., 1995). It also shows strong warming in the GIN Seas, which has been reported previously (Somavilla et al., 2013), and warming in the western Subpolar North Atlantic. Cooling trends are prominent in the deep layer in the far eastern subpolar North Atlantic, and much of the rest of the western North Atlantic. Deep and abyssal temperature variations in the North Atlantic are complex, with long-term cooling of lower NADW, but propagating decadal variations of upper NADW temperatures (Mauritzen et al., 2012), perhaps making trends a suboptimal model for deep layer temperature changes in this region. In the

rest of the ocean, there are no obvious regional deep temperature trends, just small areas of alternating signs with large magnitudes within and north of the Antarctic Circumpolar Current, and generally smaller magnitudes elsewhere.

These patterns are consistent with warming trends in the abyssal and deep layers south of 50°S (Figures 2 and 3), a weaker but still very statistically significant warming trend in the abyssal layer north of 50°S, and a still weaker warming trend in the deep layer north of 50°S. A portion of the deep layer north of 50°S shows no trend at all, between about 3,100 and 3,600 dbar. This layer includes some of the oldest waters in much of the Indian and Pacific Oceans, waters that have not been directly exposed to the surface layer for about a millennium. This bottom and southern-intensified warming pattern is apparent in high resolution ocean models, which better reproduce AABW formation (e.g., Bryan et al., 2014, their Figure 8b). Ocean heat uptake from continued reductions in AABW formation rates is projected to accelerate in the coming decades (Li et al., 2023), making the implementation of Deep Argo imperative to better monitor these changes with increased, global, and real-time sampling.

Data Availability Statement

This study used ship-based CTD data from WOD 2018 (Boyer et al., 2018) downloaded from https://www.ncei.noaa.gov/products/world-ocean-database on 2 May 2024, Deep Argo CTD data (Argo, 2024) downloaded from an Argo Global Data Assembly Center on 3 May 2024, ship-based CTD data downloaded from CCHDO (https://cchdo.ucsd.edu/) in January 2024, and ETOPO1 Bathymetry (Amante & Eakins, 2009; NOAA National Geophysical Data Center, 2009). The Gibbs-Seawater Oceanographic Toolbox (McDougall & Barker, 2011) software was also used and is available at https://www.teos-10.org/software.htm.

Acknowledgments
We thank all those who contributed to the collection, processing, quality control, and calibration of the ship-based and Deep Argo CTD data used here. Two anonymous referees made helpful comments. GCJ was supported by NOAA Global Ocean Monitoring and Observation Program and NOAA Research. SGP was supported by US Argo (NA20OAR4320278). PMEL Contribution Number 5950.

References

Amante, C., & Eakins, B. W. (2009). *ETOPO1 1 Arc-minute global relief model: Procedures, data sources and analysis*. NOAA Technical Memorandum NESDIS NGDC-24. National Geophysical Data Center, NOAA. Retrieved from https://www.ngdc.noaa.gov/mgg/global/relief/ETOPO1/docs/ETOPO1.pdf

Argo. (2024). Argo float data and metadata from global data assembly Centre (Argo GDAC). [Dataset]. *SEANOE*. https://doi.org/10.17882/42182

Boyer, T. P., Baranova, O. K., Coleman, C., Garcia, H. E., Grodsky, A., Locarnini, R. A., et al. (2018). *World Ocean Database 2018* (p. 87). A.V. Mishonov, Technical Ed., NOAA Atlas NESDIS. Retrieved from https://www.ncei.noaa.gov/sites/default/files/2020-04/wod_intro_0.pdf

Bryan, F. O., Gent, P. R., & Tomas, R. (2014). Can Southern Ocean eddy effects be parameterized in climate models? *Journal of Climate*, *27*(1), 411–425. https://doi.org/10.1175/JCLI-D-12-00759.1

Desbruyères, D. G., McDonagh, E. L., King, B. A., Garry, F. K., Blaker, A. T., Moat, B. I., & Mercier, H. (2014). Full-depth temperature trends in the northeastern Atlantic through the early 21st century. *Geophysical Research Letters*, *41*(22), 7971–7979. https://doi.org/10.1002/2014GL061844

Fogwill, C. J., Phipps, S. J., Turney, C. S. M., & Golledge, N. R. (2015). Sensitivity of the Southern Ocean to enhanced regional Antarctic ice sheet meltwater input. *Earth's Future*, *3*(10), 317–329. https://doi.org/10.1002/2015ef000306

Gunn, K. L., Rintoul, S. R., England, M. H., & Bowen, M. M. (2023). Recent reduced abyssal overturning and ventilation in the Australian Antarctic Basin. *Nature Climate Change*, *13*(6), 537–544. https://doi.org/10.1038/s41558-023-01667-8

IPCC. (2021). In V. Masson-Delmotte, P. Zhai, A. Pirani, S. L. Connors, C. Péan, et al. (Eds.), *Climate change 2021: The physical science basis. Contribution of working group I to the sixth assessment report of the intergovernmental panel on climate change* (p. 2391). Cambridge University Press. https://doi.org/10.1017/9781009157896

Johnson, G. C. (2008). Quantifying Antarctic bottom water and North Atlantic deep water volumes. *Journal of Geophysical Research*, *113*(C5), C05027. https://doi.org/10.1029/2007jc004477

Johnson, G. C. (2022). Antarctic bottom water warming and circulation slowdown in the Argentine basin from analyses of deep Argo and historical shipboard temperature data. *Geophysical Research Letters*, *49*(18), e2022GL100526. https://doi.org/10.1029/2022gl100526

Johnson, G. C., Cadot, C., Lyman, J. M., MeTaggart, K. E., & Steffen, E. L. (2020). Antarctic bottom water warming in the Brazil basin: 1990s through 2020, from WOCE to deep Argo. *Geophysical Research Letters*, *47*(18), e2020GL089191. https://doi.org/10.1029/2020gl089191

Johnson, G. C., Hosoda, S., Jayne, S. R., Oke, P. R., Riser, S. C., Roemmich, D., et al. (2022). Annual review of marine science Argo-two decades: Global oceanography, revolutionized. *Annual Review of Marine Science*, *14*(1), 379–403. https://doi.org/10.1146/annurev-marine-022521-102008

Johnson, G. C., Lyman, J. M., Boyer, T., Cheng, L., Giglio, D., Gilson, J., et al. (2024). Ocean heat content. In state of the climate in 2023, global oceans. *Bulletin of the American Meteorological Society*, *105*(8), S173–S177. https://doi.org/10.1175/BAMS-D-24-0100.1

Johnson, G. C., Lyman, J. M., & Loeb, N. G. (2016). Improving estimates of Earth's energy imbalance. *Nature Climate Change*, *6*(7), 639–640. https://doi.org/10.1038/nclimate3043

Johnson, G. C., Lyman, J. M., & Purkey, S. G. (2015). Informing deep Argo array design using Argo and full- depth hydrographic section data. *Journal of Atmospheric and Oceanic Technology*, *32*(11), 2187–2198. https://doi.org/10.1175/JTECH-D-15-0139.1

Johnson, G. C., Purkey, S. G., & Toole, J. M. (2008). Reduced Antarctic meridional overturning circulation reaches the North Atlantic ocean. *Geophysical Research Letters*, *35*(22), L22601. https://doi.org/10.1029/2008gl035619

Johnson, G. C., Purkey, S. G., Zilberman, N. V., & Roemmich, D. (2019). Deep Argo quantifies bottom water warming rates in the Southwest Pacific basin. *Geophysical Research Letters*, *46*(5), 2662–2669. https://doi.org/10.1029/2018gl081685

Kouketsu, S., Doi, T., Kawano, T., Masuda, S., Sugiura, N., Sasaki, Y., et al. (2011). Deep ocean heat content changes estimated from observation and reanalysis product and their influence on sea level change. *Journal of Geophysical Research*, *116*(16), C03012. https://doi.org/10.1029/2010jc006464

Li, Q., England, M. H., Hogg, A. M., Rintoul, S. R., & Morrison, A. K. (2023). Abyssal ocean overturning slowdown and warming driven by Antarctic meltwater. *Nature*, *615*(7954), 841–847. https://doi.org/10.1038/s41586-023-05762-w

Masuda, S., Awaji, T., Sugiura, N., Matthews, J. P., Toyoda, T., Kawai, Y., et al. (2010). Simulated rapid warming of abyssal North Pacific waters. *Science*, *329*(5989), 319–322. https://doi.org/10.1126/science.1188703

Mauritzen, C., Melsom, A., & Sutton, R. (2012). Importance of density-compensated temperature change for deep North Atlantic Ocean heat uptake. *Nature Geoscience*, *5*(12), 905–910. https://doi.org/10.1038/ngeo1639

McDougall, T. J., & Barker, P. M. (2011). Getting started with TEOS-10 and the gibbs seawater (GSW) oceanographic toolbox, SCOR/IAPSO WG127 28.

NOAA National Geophysical Data Center. (2009). ETOPO1 1 Arc-minute global relief model. [Dataset]. *NOAA National Centers for Environmental Information*. https://doi.org/10.7289/V5C8276M

Orsi, A. H., Whitworth, T., & Nowlin, W. D. (1995). On the meridional extent and fronts of the Antarctic circumpolar current. *Deep Sea Research Part I: Oceanographic Research Papers*, *42*(5), 641–673. https://doi.org/10.1016/0967-0637(95)00021-w

Purkey, S. G., & Johnson, G. C. (2010). Warming of global abyssal and deep Southern Ocean waters between the 1990s and 2000s: Contributions to global heat and sea level rise budgets. *Journal of Climate*, *23*(23), 6336–6351. https://doi.org/10.1175/2010jcli3682.1

Purkey, S. G., Johnson, G. C., Talley, L. D., Sloyan, B. M., Wijffels, S. E., Smethie, W., et al. (2019). Unabated bottom water warming and freshening in the South Pacific ocean. *Journal of Geophysical Research-Oceans*, *124*(3), 1778–1794. https://doi.org/10.1029/2018jc014775

Roemmich, D., Alford, M. H., Claustre, H., Johnson, K., King, B., Moum, J., et al. (2019). On the future of Argo: A global, full-depth, multi-disciplinary array. *Frontiers in Marine Science*, *6*(439). https://doi.org/10.3389/fmars.2019.00439

Silvano, A., Purkey, S., Gordon, A. L., Castagano, P., Stewart, A. L., Rintoul, S. R., et al. (2023). Observing Antarctic bottom water in the Southern Ocean. *Frontiers in Marine Science*, *10*, 122701. https://doi.org/10.3389/fmars.2023.1221701

Sloyan, B. M., Wanninkhof, R., Kramp, M., Johnson, G. C., Talley, L., Tanhua, T., et al. (2019). The Global Ocean ship-base hydrographic investigations Program (GO-SHIP): A platform for integrated multidisciplinary ocean science. *Frontiers in Marine Science*, *6*(445). https://doi.org/10.3389/fmars.2019.00445

Somavilla, R., Schauer, U., & Budeus, G. (2013). Increasing amount of Arctic Ocean Deep waters in the Greenland sea. *Geophysical Research Letters*, *40*(16), 4361–4366. https://doi.org/10.1002/grl.50775

Storto, A., Cheng, L. J., & Yang, C. X. (2022). Revisiting the 2003-18 deep ocean warming through multiplatform analysis of the global energy budget. *Journal of Climate*, *35*(14), 4701–4717. https://doi.org/10.1175/jcli-d-21-0726.1

Tukey, J. W. (1977). *Exploratory data analysis*. Addison-Wesley. OCLC 3058187.

Volkov, D. L., Lee, S.-K., Landerer, F. W., & Lumpkin, R. (2017). Decade-long deep-ocean warming detected in the subtropical South Pacific. *Geophysical Research Letters*, *44*(2), 927–936. https://doi.org/10.1002/2016GL071661

von Schuckmann, K., Minière, A., Gues, F., Cuesta-Valero, F. J., Kirchengast, G., Adusumilli, S., et al. (2023). Heat stored in the Earth system 1960-2020: Where does the energy go? *Earth System Science Data*, *15*(4), 1675–1709. https://doi.org/10.5194/essd-15-1675-2023

Wunsch, C., & Heimbach, P. (2014). Bidecadal thermal changes in the abyssal ocean. *Journal of Physical Oceanography*, *44*(8), 2013–2030. https://doi.org/10.1175/jpo-d-13-096.1

Yashayaev, I., & Loder, J. W. (2016). Recurrent replenishment of Labrador Sea Water and associated decadal-scale variability. *Journal of Geophysical Research-Oceans*, *121*(11), 8095–8114. https://doi.org/10.1002/2016jc012046

Zhou, S., Meijers, A. J. S., Meredith, M. P., Abrahamson, E. P., Holland, P. R., Silvano, A., et al. (2023). Slowdown of Antarctic Bottom Water export driven by climatic wind and sea-ice changes. *Nature Climate Change*, *13*(7), 701–709. https://doi.org/10.1038/s41558-023-01695-4

Zilberman, N. V., Thierry, V., King, B., Alford, M., Andre, X., Balem, K., et al. (2023). Observing the full ocean volume using Deep Argo floats. *Frontiers in Marine Science*, *10*. https://doi.org/10.3389/fmars.2023.1287867